The X–θ Framework: Geometry, Analogies, Math, and Where It Bites Physics

A Unified Non-Relativistic and Relativistic Formulation on $Q = \mathbb{R}^{3,1} \times S^1$

Divyang Panchasara

DRAFT — 14 Sep 2025

Contents

Abstract

Imagine our universe has an extra hidden dimension shaped like a circle. In the X–θ framework, this compact angle θ is added to ordinary space–time, with the goal of unifying familiar forces like electromagnetism and gravity through a simple geometric idea. I show how this extra dimension influences physical phenomena from electromagnetic fields to quantum mechanics, and I outline clear, testable signatures: phase shifts at zero electromagnetic fields (a θ–Aharonov–Bohm effect), near-harmonic "rotor" sidebands with spacing set by the phase inertia, and correlated short-range Yukawa deviations across sectors in a simple Stueckelberg completion. I also connect to cosmology, where the extra degree of freedom behaves as a stiff component and can help regularize singular behavior. Finally, I propose concrete laboratory and astrophysical tests, making the framework not only intriguing but also falsifiable.

1 Overview (Steering by Phase: A Quick Tour)

Picture ordinary motion as the wheels of a car and θ as a small, hidden steering column geared to them. Even on a perfectly flat road (no EM fields), turning the hidden column and coming back to where you started leaves a loop holonomy that interferometers can read. If the gear ratio varies across space (mixed curvature $G_{\mu\theta}$), the car drifts sideways (a cross-Hall response). The dial is periodic: turn it by 2π and the effects repeat.

Three lab anchors: (i) θ–Aharonov–Bohm at $\mathbf{E} = \mathbf{B} = 0$, (ii) cross-Hall drift from $\partial_i A_\theta$, and (iii) rotor sidebands with spacing $\Delta E \approx \hbar^2/(2I)$.

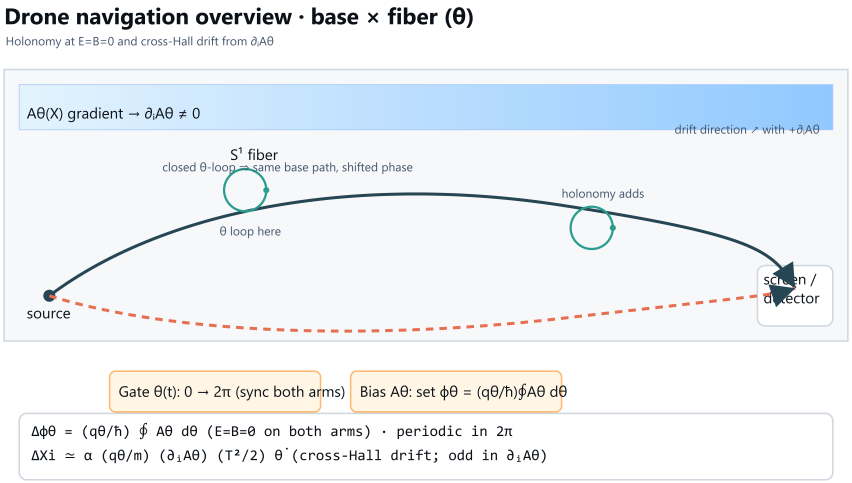

Figure 1: Drone navigation analogy: base motion (drone) with an internal θ dial (orange). Closing a loop on the dial leaves a holonomy ϕ_θ visible at $\mathbf{E} = \mathbf{B} = 0$; blue arrows illustrate cross-Hall drifts when $\partial_\mu A_\theta \neq 0$.

Pointers: lab holonomy (section 3.1), sidebands as an inertia gauge (section 3.3), unified range (section 7), and bounce/WDW barrier (section 4).

2 The X–θ Mathematical Framework (Central Formalism)

I collect the full formalism here; later sections specialize to experiments and cosmology. To match prior drafts that used F_{ab}, I write the field strength on Q as $G_{ab} \equiv \partial_a A_b - \partial_b A_a$ (synonymous with F_{ab} earlier).

Units and conventions. Unless stated otherwise, I use SI units in this section and keep $\hbar$ explicit in quantum contexts. In the relativistic Stueckelberg completion (section 7) I adopt natural units with $\hbar = c = 1$; when needed, $\hbar$ and c can be restored by dimensional analysis.

2.1 Configuration space, connection, and curvature

$$Q = \mathbb{R}^{3,1} \times S^1, \qquad q^a = (X^\mu, \theta), \qquad a \in \{0, 1, 2, 3, \theta\}, \tag{1}$$

$$A = A_a\, dq^a = A_\mu\, dX^\mu + A_\theta\, d\theta, \qquad G = dA, \qquad G_{ab} = \partial_a A_b - \partial_b A_a. \tag{2}$$

Key mixed component: $G_{\mu\theta} = \partial_\mu A_\theta - \partial_\theta A_\mu$.

Idea in one line. Think of ordinary space as a city map, and add a tiny circular *dial* θ at every point. Turning the dial moves you along the fiber circle without moving on the map. The connection A tells you how "phase" changes as you move—on the map and around the dial. The curvature $G = dA$ measures how those changes *fail to cancel* around a loop (that failure is the holonomy). A picture of this "map × dial" view is shown in Fig. 2.

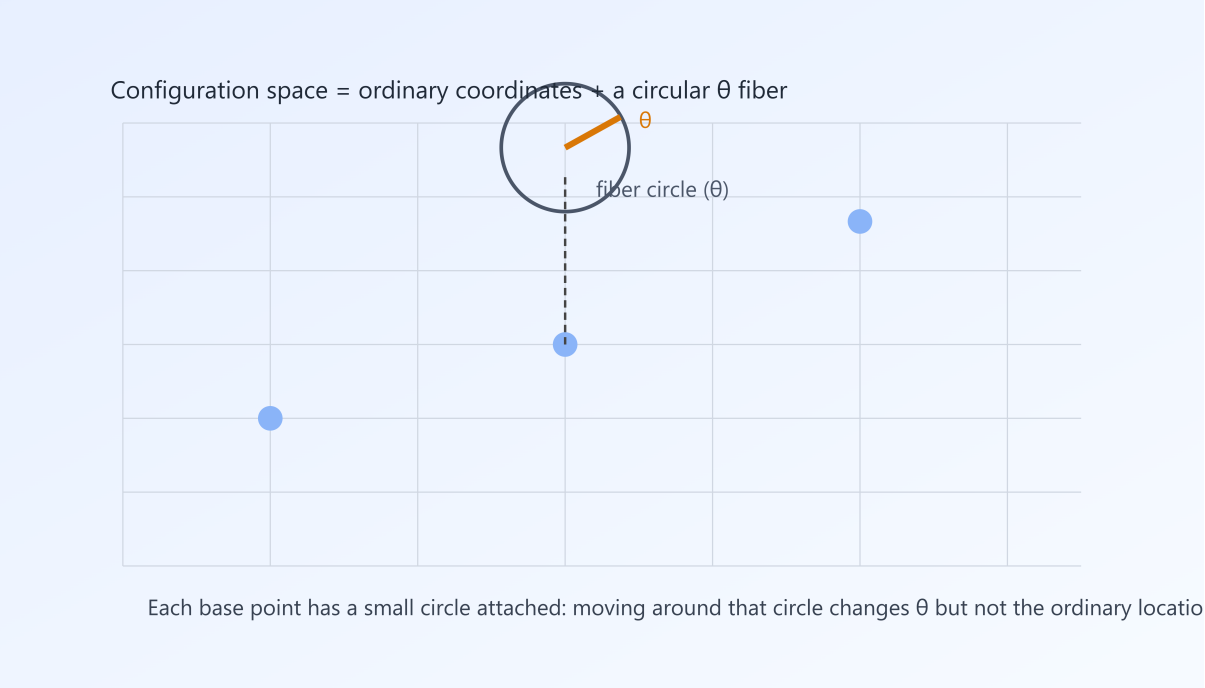

Figure 2: Configuration space as "map × dial": every base point carries a circular fiber θ. Mixed curvature $G_{\mu\theta}$ links base motion to the fiber dial.

Intuition and analogies.

- **Compact dimension (S^1).** $Q = \mathbb{R}^{3,1} \times S^1$ means I add one extra circular coordinate θ (angle, period 2π) to ordinary space–time. Analogy: a garden hose looks 1D from afar but has a circular cross-section up close.
- **Gauge connection (A).** A geometric bookkeeping tool for how phases change when you move: a 1-form $A = A_a dq^a = A_\mu dX^\mu + A_\theta d\theta$. Analogy: a boat's navigation aid compensating for currents so transport is consistent.

- **Curvature ($G = dA$) and holonomy.** Curvature measures the failure of phase changes to cancel on a loop; holonomy is the loop-induced phase. Analogy: hike a loop around a hill and your compass heading can twist.
- **Mixed curvature ($G_{\mu\theta}$).** Couples base motion and internal rotation; in the common gauge $\partial_\theta A_\mu = 0$ this reduces to a spatial gradient $\partial_\mu A_\theta$ that produces the cross-Hall response. Analogy: meshed gears—motion in one drives the other.

2.2 Non-relativistic Lagrangian, Hamiltonian, and currents

With Newtonian time t and $\phi \equiv A_0$,

$$L_{\rm NR} = \frac{m}{2}\dot{X}^2 + \frac{I}{2}\dot{\theta}^2 + q_X A_i \dot{X}^i + q_\theta A_\theta \dot{\theta} - q_X\,\phi, \tag{3}$$

$$P_i = m\dot{X}^i + q_X A_i, \quad p_\theta = I\dot{\theta} + q_\theta A_\theta. \tag{4}$$

Equations of motion:

$$m\ddot{X}_i = q_X\,(E_i + (\dot{\boldsymbol{X}} \times \boldsymbol{B})_i) + q_\theta\, G_{i\theta}\,\dot{\theta}, \tag{5}$$

$$I\ddot{\theta} = q_\theta\, G_{\theta 0} + q_\theta\, G_{\theta i}\,\dot{X}^i, \tag{6}$$

with $E_i = -\partial_t A_i - \partial_i \phi$ and $\boldsymbol{B} = \nabla \times \boldsymbol{A}$. Quantum dynamics on Q:

$$i\hbar\,\partial_t \psi = \left[\frac{1}{2m}(-i\hbar\nabla_X - q_X \boldsymbol{A})^2 + \frac{1}{2I}(-i\hbar\partial_\theta - q_\theta A_\theta)^2 + q_X\,\phi\right]\psi. \tag{7}$$

Continuity on Q:

$$\partial_t \rho + \nabla_X \cdot \boldsymbol{J}_X + \partial_\theta J_\theta = 0, \tag{8}$$

$$\boldsymbol{J}_X = \frac{1}{m}\,\mathrm{Re}[\psi^\dagger(-i\hbar\nabla_X - q_X\boldsymbol{A})\psi], \quad J_\theta = \frac{1}{I}\,\mathrm{Re}[\psi^\dagger(-i\hbar\partial_\theta - q_\theta A_\theta)\psi]. \tag{9}$$

Idea in one line. A Lagrangian is a *trip budget*: kinetic terms are fuel costs (base and θ motion), potentials are hills, and the gauge potentials (A_i, A_θ) act like tolls that depend on where and how you move. The Hamiltonian is the accountant: it doesn't let energy vanish, it just allows it to move between base motion, fiber motion, and interactions. A single units reminder keeps this honest: $[A_\theta] = \hbar/q_\theta$, so $q_\theta A_\theta$ carries momentum units along θ.

Units sanity (quick check).

- $[A_\theta] = \hbar/q_\theta$ so that $q_\theta A_\theta$ carries momentum units along θ; $[\partial_i A_\theta] = (\hbar/q_\theta)/\text{length}$.
- The Lagrangian piece $q_\theta A_\theta\,\dot{\theta}$ has energy units; the cross-Hall force term $q_\theta(\partial_i A_\theta)\,\dot{\theta}$ has force units.

Reading the Hamiltonian (at a glance).

- Minimal coupling: $\boldsymbol{p} \to \boldsymbol{p} - q_X\boldsymbol{A}$ and $p_\theta \to p_\theta - q_\theta A_\theta$ incorporate forces via potentials.
- Two kinetic energies describe base and fiber motion: $\frac{1}{2m}(\cdots)^2$ and $\frac{1}{2I}(\cdots)^2$. The parameter I is an internal moment of inertia.
- Continuity on Q is just probability conservation on the enlarged space.

EP hygiene (assumption). To avoid composition-dependent violations of the equivalence principle at leading order, I take the θ-charge to be composition-independent (e.g., $Q_\theta = \beta m$ or $\propto B-L$). This makes the new force universal at first approximation and is consistent with Eötvös-type constraints; any residual composition dependence then only arises via the tiny portal mixings in section 7.

Rotor spectrum and holonomy shift:

$$E_\ell = \frac{\hbar^2}{2I}\Big(\ell - \frac{\phi_\theta}{2\pi}\Big)^2, \qquad \phi_\theta \equiv \frac{q_\theta}{\hbar}\oint A_\theta\, d\theta, \qquad \ell \in \mathbb{Z}. \tag{10}$$

2.3 Relativistic worldline, massless limit, and covariant wave equation

Worldline action with einbein $e(\tau)$ and metric $G^{(\mathrm{geom})}_{ab}dq^a dq^b = \eta_{\mu\nu}dX^\mu dX^\nu + \kappa^2 d\theta^2$:

$$S_{\mathrm{rel}} = \int d\tau\Big[\frac{1}{2e}\,G^{(\mathrm{geom})}_{ab}\,\dot q^a \dot q^b - \frac{e}{2}\,m^2 + q_X A_\mu \dot X^\mu + q_\theta A_\theta \dot\theta\Big]. \tag{11}$$

Mass-shell constraint $G^{ab}_{(\mathrm{geom})}(P_a - q_a A_a)(P_b - q_b A_b) + m^2 = 0$. In the NR limit $I = m\kappa^2$.

Worldline and einbein (at a glance).

- The path is parametrized by τ; the einbein $e(\tau)$ keeps the action reparametrization-invariant.
- Varying e enforces the mass-shell condition that reduces to $E^2 = \boldsymbol{p}^2 + m^2$ when fields vanish.
- The added metric piece $\kappa^2 d\theta^2$ says motion in θ contributes to the worldline length; in the NR limit one finds $I = m\kappa^2$.
- Intuition: the einbein is like a choice of speedometer; it sets the clock along the path without changing the trip.

Covariant wave equation on Q (scalar):

$$\left[D_\mu D^\mu + \kappa^{-2} D_\theta^2 + m^2\right]\Psi(X,\theta) = 0, \quad D_\mu = \partial_\mu + \tfrac{i}{\hbar} q_X A_\mu,\ D_\theta = \partial_\theta + \tfrac{i}{\hbar} q_\theta A_\theta. \tag{12}$$

Massless limit ($m \to 0$). With finite κ_0,

$$S_{m=0} = \int d\tau\Big[\frac{1}{2e}(\eta_{\mu\nu}\dot X^\mu \dot X^\nu + \kappa_0^2\dot\theta^2) + q_X A_\mu \dot X^\mu + q_\theta A_\theta \dot\theta\Big], \quad \eta_{\mu\nu}\dot X^\mu \dot X^\nu + \kappa_0^2\dot\theta^2 = 0. \tag{13}$$

NR map. Removing the rest-energy phase yields the Schrödinger equation in section 2.2 provided I identify $\boxed{I = m\kappa^2}$.

Idea in one line. Two pictures: the *rubber sheet* (curvature makes dimples that steer motion) and the *ripple* (the covariant wave equation moves ripples consistently in any good coordinates). The fiber just adds one compact direction the ripple can wrap around; the NR limit packages it into the rotor inertia $I = m\kappa^2$.

Parameter map. The rotor inertia I is a probe property tied to geometry via $I = m\kappa^2$, whereas the 4D vector mass $m_\theta = g_\theta f_\theta$ in the Stueckelberg completion is a mediator property controlling the shared Yukawa range $\lambda_\theta = 1/m_\theta$ (section 7).

2.4 Gauge invariance on Q and large loops

Gauge transformations: $A_\mu \to A_\mu + \partial_\mu \Lambda_X$, $A_\theta \to A_\theta + \partial_\theta \Lambda_\theta$, with $\psi \to \exp\left[-\frac{i}{\hbar}(q_X \Lambda_X + q_\theta \Lambda_\theta)\right] \psi$. Under a large gauge transformation around the circle, $\oint A_\theta d\theta \to \oint A_\theta d\theta + 2\pi\,\hbar/q_\theta$, so only ϕ_θ modulo 2π is physical.

Idea in one line. Changing gauge is like moving the zero mark on an altimeter: the mountain stays the same. Only *closed loops* reveal structure. March once around the fiber circle and you collect a net phase $\phi_\theta = \frac{q_\theta}{\hbar} \oint A_\theta d\theta$, but physics cares only modulo 2π (large–gauge periodicity).

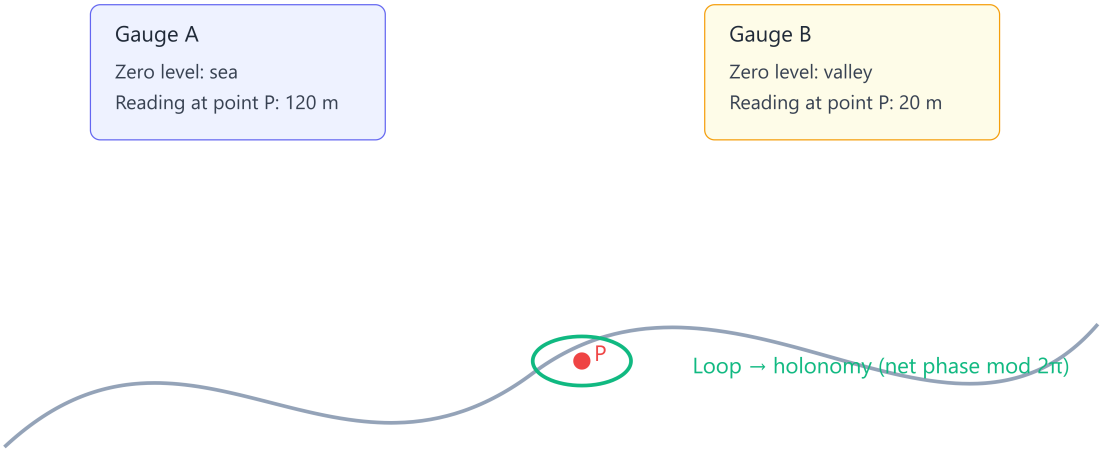

Figure 3: Gauge change shifts the reference, not the hill. A closed loop probes holonomy; only ϕ_θ
$bmod 2\pi$ is observable.

The Bianchi identity $dG = 0$ holds for $G = dA$ when one treats (A_μ, A_θ) as components of a single connection; in many experiments I choose $\partial_\theta A_\mu = 0$, leaving the measurable gradient $\partial_\mu A_\theta$.

2.5 Consistency checks & known limits

- **Turning off the fiber ($I \to \infty$, $q_\theta \to 0$).** Dynamics reduce to standard electrodynamics and quantum mechanics on $\mathbb{R}^{3,1}$: no A_θ phases and no rotor sidebands.
- **Turning off base electromagnetism ($q_X \to 0$).** The system is a free internal rotor that can still depend on X through $A_\theta(X)$; sidebands with spacing $\Delta E \approx \hbar^2/(2I)$ and the θ–AB phase $\Delta\varphi_\theta = \frac{q_\theta}{\hbar} \oint A_\theta d\theta$ persist.
- **Relativistic $\to$ non-relativistic.** Identifying $I = m\kappa^2$ ensures the Schrödinger equation inherits the correct rotor term $\frac{1}{2I}(-i\hbar\partial_\theta - q_\theta A_\theta)^2$ after removing the rest-energy phase.

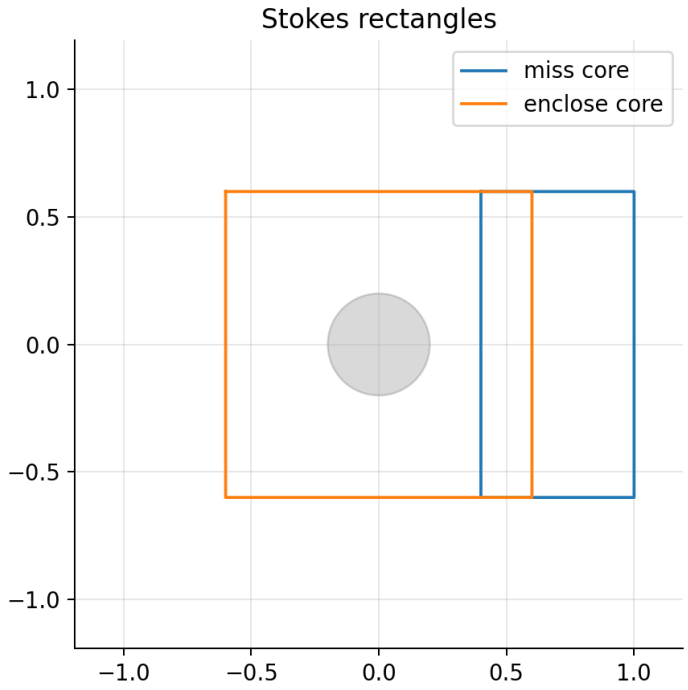

Figure 4: Holonomy schematic: Stokes rectangles visualize how loop integrals relate to enclosed curvature; only the loop integral modulo the large-gauge period is observable.

2.6 Worked reductions (one screen)

I summarize the $I \to \infty$, $q_X \to 0$, and $I = m\kappa^2$ limits and their outcomes for observables (sidebands, holonomy) and consistency.

3 Phenomena & Tests (Lab and Null-EM Signatures)

Convention: "Fiber-off" means $I \to \infty$ and $q_\theta \to 0$.

3.1 θ–AB phase under null spatial fields

Action contribution along a closed internal loop $\mathcal{C}_\theta$ yields a path-integral phase $\exp[i(q_\theta/\hbar) \oint A_\theta d\theta]$. The observable phase is

$$\Delta\varphi_\theta = \frac{q_\theta}{\hbar} \oint A_\theta \, d\theta \pmod{2\pi}, \qquad \boldsymbol{E} = \boldsymbol{B} = 0. \tag{14}$$

Idea in one line. Like a note sounding different in two rooms, the *phase* can shift even when $\mathbf{E} = \mathbf{B} = 0$ along both arms. Here the hidden dial θ supplies the shift: $\Delta\varphi = \phi_\theta \pmod{2\pi}$, so sweeping ϕ_θ by 2π brings the fringes right back.

Data: `../paper/data/exp1_theta_ab_fringe.csv`.

Support visuals: AB baseline (`ab_baseline.png`) and vector-field paths (`avec_quiver_paths.png`).

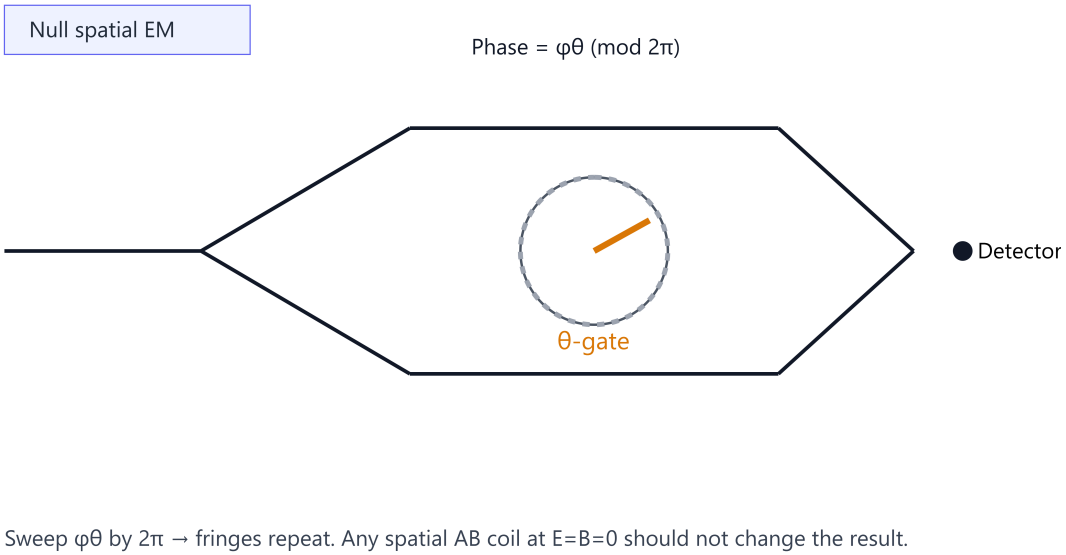

Figure 5: θ–AB interferometer at null spatial EM. The θ-gate dials ϕ_θ; fringes are strictly 2π-periodic.

3.2 Cross-Hall drift from mixed curvature

With $\boldsymbol{E} = \boldsymbol{B} = 0$, $m\ddot{X}_i = q_\theta\, G_{i\theta}\, \dot{\theta}$ ($G_{i\theta} = \partial_i A_\theta - \partial_\theta A_i$). For a uniform gate of duration T and nearly constant $\dot{\theta}$,

$$\Delta X_i \simeq \alpha\, \frac{q_\theta}{m}\, (\partial_i A_\theta)\, \frac{T^2}{2}\, \dot{\theta}, \qquad \alpha \lesssim 1. \tag{15}$$

Idea in one line. A hidden current can push a boat sideways. Likewise a gradient $\partial_y A_\theta$ plus a time window with $\dot{\theta} \neq 0$ nudges the packet: $\Delta y \propto (\partial_y A_\theta)\, \dot{\theta}\, T^2$. Flip either sign and the drift reverses; turn either off and it vanishes.

Data: `../paper/data/exp2_drift_T2.csv`.

3.3 Sidebands from the rotor Hamiltonian

Separating variables $\Psi = \sum_\ell \psi_\ell(X) e^{i\ell\theta}$ yields rotor levels $E_\ell = \frac{\hbar^2}{2I}(\ell - \phi_\theta/2\pi)^2$ and nearest-neighbor spacing $\Delta E \approx \hbar^2/(2I)$.

Data: `../paper/data/exp3_rotor_levels.csv`.

3.4 Order-of-magnitude anchors for I

$\Delta E = h\,\Delta f$, $I \approx \hbar^2/(2\,\Delta E)$. Example: $\Delta f = 1\,\mathrm{Hz} \Rightarrow I \approx 8.4 \times 10^{-36}\,\mathrm{J\,s^2}$.

3.5 Falsification protocol

Vary spatial flux at fixed ϕ_θ; enforce 2π periodicity in ϕ_θ; use closed θ-loop controls and arm swaps.

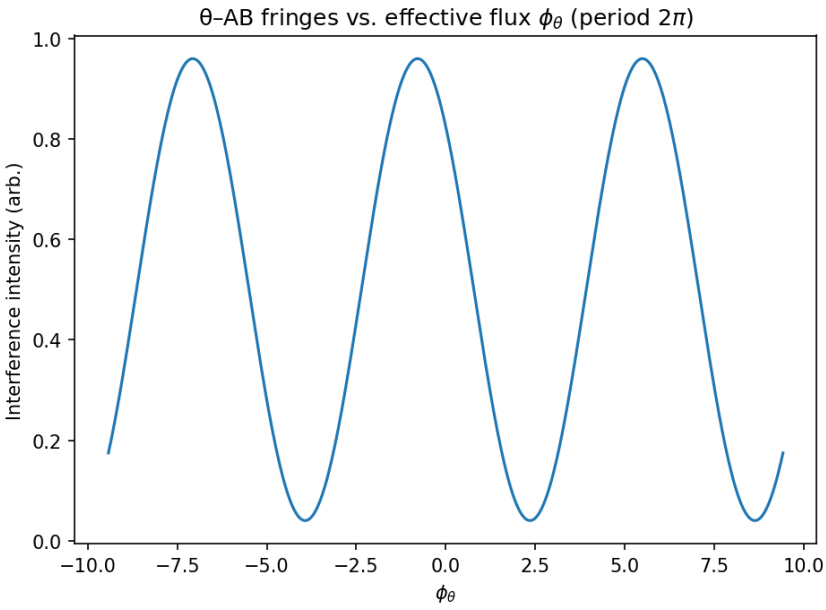

Figure 6: Fringe vs. ϕ_θ (simulation).

3.6 Consistency checks & limits (QM/NR)

Fiber-off ($I \to \infty$, $q_\theta \to 0$), pure θ sector ($q_X \to 0$), large-gauge periodicity in $\oint A_\theta d\theta$.

3.7 Methods: θ–Aharonov–Bohm interferometer

Program a $\theta(t)$ modulation that advances by $2\pi N_\theta$ during the arm transit; if A_θ is approximately constant along the path in θ, then $\Delta\varphi_\theta \approx (q_\theta/\hbar)A_\theta(2\pi N_\theta)$.

3.8 Mesoscopic Transport: AB Rings with a θ-Flux Offset

$G(\Phi, \Phi_\theta) \propto \cos[2\pi(\Phi/\Phi_0 + \Phi_\theta/\Phi_{\theta,0})]$, $\Phi_{\theta,0} = 2\pi\hbar/q_\theta$.

3.9 Singularity seam: where classical GR fails and QM fixes

Classical FRW: stiff a^{-6} alone doesn't bounce; adding curvature ($-k/a^2$ with $k > 0$) creates a turning point. Wheeler–DeWitt adds a repulsive $+C/a^2$ barrier that blocks $a \to 0$.

Experimental Details, SNR, and Error Budgets

Interferometric phase @ null spatial EM (θ–AB)

Signal model. $I(\phi_\theta) = \frac{1}{2}[1 + V\cos(\phi_\theta + \phi_0)]$ with visibility $V \in [0, 1]$. For N detected quanta per point, the shot-noise limited phase uncertainty is $\sigma_\phi \approx 1/\sqrt{NV^2}$ (small-angle, high-contrast). I sweep $\phi_\theta \in [-4\pi, 4\pi]$.

extbfFalsification gate. A 2π-periodic fit must achieve reduced $\chi^2 \lesssim 1.5$ and circular-variance of residuals $< 0.1\,\mathrm{rad}^2$; dependence on any spatial AB toggle at $E{=}B{=}0$ must be $< 2\sigma$ of shot noise.

Data: `../paper/data/exp1_theta_ab_fringe.csv`.

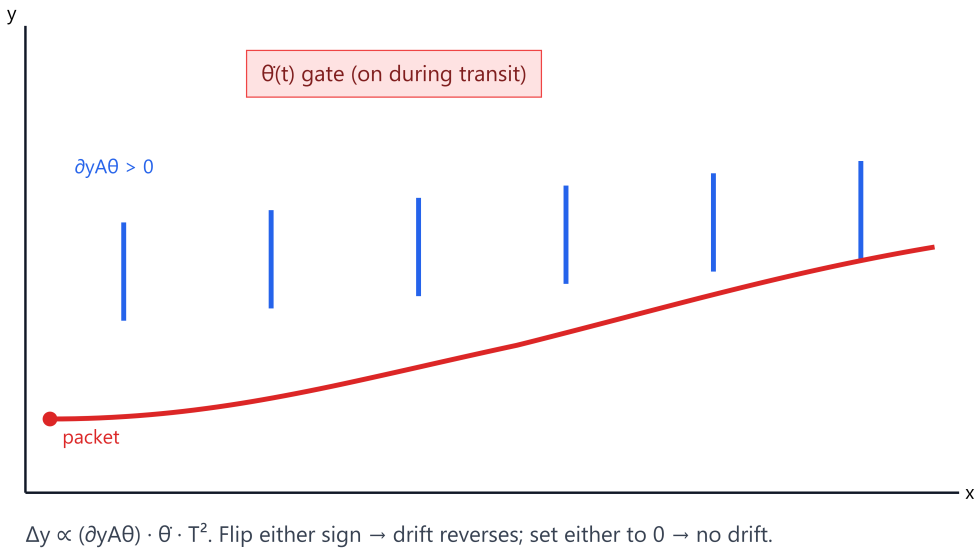

Figure 7: Cross–Hall drift intuition: blue arrows for $\partial_y A_\theta$, red packet deflection.

Cross–Hall drift

Signal model. $\Delta y = \alpha\,(\partial_y A_\theta)\,\dot{\theta}\,T^2$. Reverse either $\partial_y A_\theta$ or $\dot{\theta} \Rightarrow \Delta y \to -\Delta y$.

extbfUncertainty. Centroid error $\sigma_y \simeq w/\sqrt{N}$ (spot size w); slope uncertainty from linear fit of Δy vs T^2. extbfFalsification gate. $R^2(\Delta y \text{ vs } T^2) > 0.95$ *and* correct sign flips; otherwise reject.

Data: `../paper/data/exp2_drift_T2.csv`.

Rotor sidebands

extbfSignal model. $E_\ell = \frac{\hbar^2}{2I}\left(\ell - \frac{\phi_\theta}{2\pi}\right)^2$. extbfFit. Quadratic fit residual RMS $< \frac{1}{3}$ linewidth; holonomy shift periodic in 2π.

Data: `../paper/data/exp3_rotor_levels.csv`.

Bounce and shared-range tests

$a_{\min} = \left[(A + \Sigma^2)/k\right]^{1/4}$ with $A = \frac{8\pi G}{3}\,\frac{\Pi_\theta^2}{2I_0}$.

Data: `../paper/data/exp4_bounce_scan.csv`.,

Data: `../paper/data/exp5_yukawa_profiles.csv`.

4 Cosmology Link — From Minisuperspace to a Bounce

I sketch classical and quantum pictures in a spatially flat FRW minisuperspace with scale factor $a(t)$ and homogeneous $\theta(t)$.

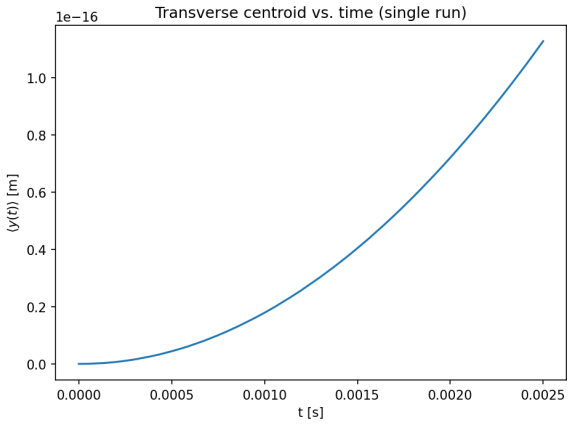

(a) Centroid trajectory $\langle y(t)\rangle$

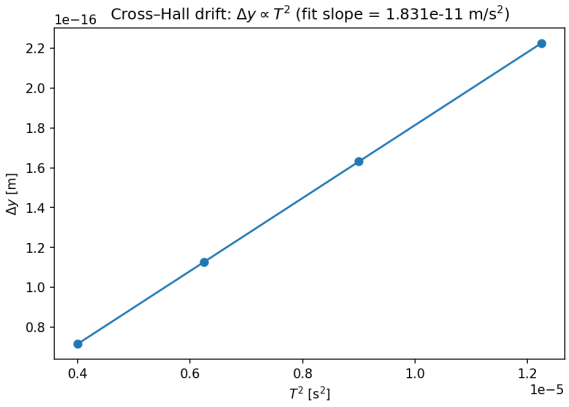

(b) Δy vs T^2 scaling

Figure 8: Cross–Hall drift: simulation traces and T^2 scaling.

4.1 Choice of I: FRW (stiff) vs. WDW (barrier)

For FRW, take $I = I_0$ (constant). Then

$$\rho_\theta(a) = \frac{\Pi_\theta^2}{2I_0\, a^6}, \qquad \Pi_\theta \equiv a^3\,(I_0\,\dot\theta + q_\theta A_\theta) = \text{const}, \quad w = 1. \tag{16}$$

For WDW, separating $\Psi = \chi(a)e^{i\ell\theta}$ gives a repulsive inverse-square barrier $+\ell^2\hbar^2/(2I_0a^2)$.

4.2 Classical bounce (self-balanced a^{-6} and effective potential)

Early-time Friedmann with positive shear-like piece $+\Sigma^2/a^6$ and curvature $-k/a^2$ ($k > 0$):

$$H^2 = \frac{8\pi G}{3}\left(\rho_{\rm std} + \frac{\Pi_\theta^2}{2I_0\, a^6}\right) + \frac{\Sigma^2}{a^6} - \frac{k}{a^2}\,. \tag{17}$$

Defining $A \equiv \frac{8\pi G}{3}\frac{\Pi_\theta^2}{2I_0}$ and neglecting $\rho_{\rm std}$ at early times,

$$H^2 = \frac{A+\Sigma^2}{a^6} - \frac{k}{a^2}, \qquad a_{\rm min} = \left(\frac{A+\Sigma^2}{k}\right)^{1/4}. \tag{18}$$

Data: `../paper/data/exp4_bounce_scan.csv`.

4.3 Wheeler–DeWitt (quantum) wall at $a = 0$

Separation $\Psi(a,\theta) = \chi(a)e^{i\ell\theta}$ gives

$$\left[-\partial_a^2 + U(a) + \frac{\ell^2\hbar^2}{2I_0a^2}\right]\chi(a) = 0, \tag{19}$$

so the $+C/a^2$ term (with $C \propto \ell^2\hbar^2/I_0$) is a repulsive inverse-square barrier. Appropriate boundary conditions (or limit-point behavior for large enough C) yield a self-adjoint Hamiltonian and unitary evolution.

5 Simulation Playbook (Minimal Viable Demos)

Grid-based split-step evolution of a Gaussian packet on (x, y) with a discrete θ ladder demonstrates cross-Hall drift and θ–AB phases. Key readouts: centroid drift $\langle y(t)\rangle$, interferometric phase vs. $\oint A_\theta d\theta$, and Fourier spectra showing $\Delta E \approx \hbar^2/(2I)$.

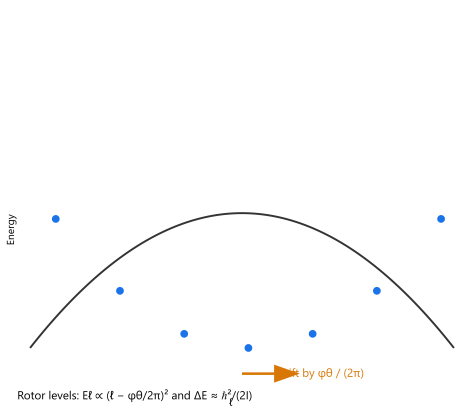

(a) Rotor levels (cartoon)

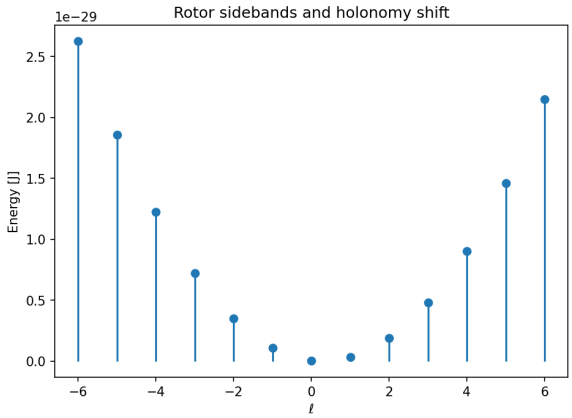

(b) Rotor levels (simulation)

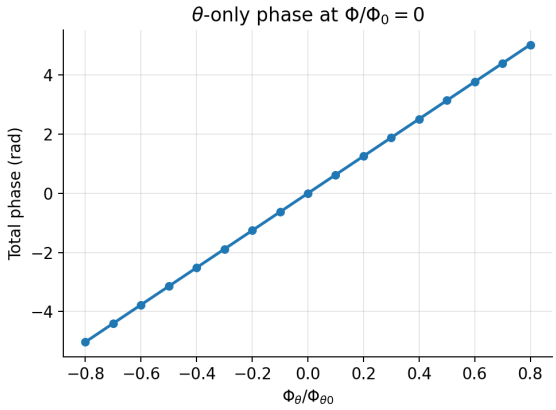

(c) θ-only baseline

Figure 9: Rotor sidebands and θ-only baseline.

Simulation Assumptions & Limitations

Numerics. Split–step propagation on (x, y); internal rotor treated via fixed Fourier index ℓ. Time step satisfies the spatial CFL bound. Grids: $N_x{=}N_y$ (reported per run).
Physics scope. No interparticle interactions; no decoherence or technical noise; classical $A_\theta(t, y)$ profiles; no back-reaction on θ dynamics.
Boundaries. Periodic in x, y for FFT (packet remains well inside domain).
Validation. Code reproduces free-packet propagation and agrees with analytic T^2 drift scaling for linear A_θ gradients within numeric error.
Implication. Sim results demonstrate *internal consistency* and *detectability estimates*; they are not substitutes for measured data in the proposed setups.

6 Reserved — Open for Future Extensions

This placeholder reserves numbering continuity for a future section (e.g., condensed-matter analogs or extended data).

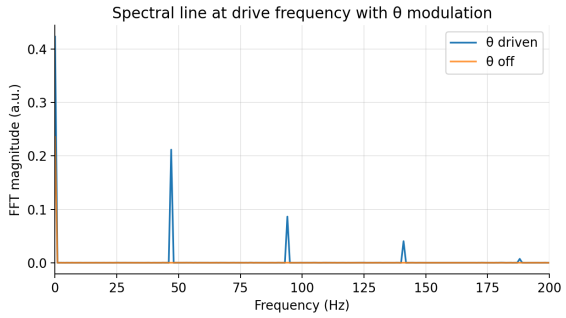

(a) FFT of a sample θ drive

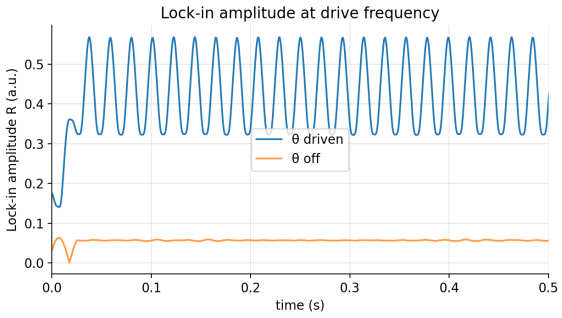

(b) Lock-in demodulation concept

Figure 10: Method visuals for θ–AB interferometry.

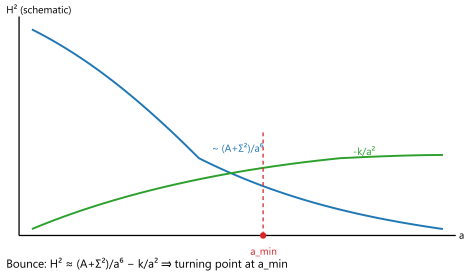

(a) Bounce schematic

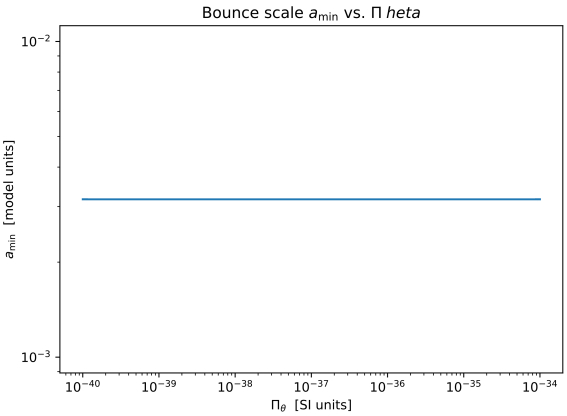

(b) Bounce scan (simulation)

Figure 11: Classical bounce: schematic and simulation turning point.

7 Unified Force — Fixed-Core (Stueckelberg) Edition

I promote the fiber angle to a 4D field $\Theta(x)$ and the fiber connection to a 4D gauge field $A_{\theta\mu}(x)$. A Stueckelberg mass $m_\theta = g_\theta f_\theta$ gives a single Yukawa range $\lambda_\theta = 1/m_\theta$.

7.1 From Q to 4D: fields and covariant derivatives

Pullback of the connection on $Q = \mathbb{R}^{3,1} \times S^1$: $\Theta(x)$ and $A_{\theta\mu}(x)$. $D_\mu\Theta = \partial_\mu\Theta - g_\theta A_{\theta\mu}$; for matter, $D_\mu\psi = (\cdots + i g_\theta Q_\theta A_{\theta\mu})\psi$.

7.2 Lagrangian core and mass

$$\mathcal{L} \supset -\tfrac{1}{4} F^{(\theta)}_{\mu\nu} F^{\mu\nu}_{(\theta)} + \frac{f_\theta^2}{2}\,(\partial_\mu\Theta - g_\theta A_{\theta\mu})^2 - \frac{\varepsilon_Y}{2}\, F^{(\theta)}_{\mu\nu} B^{\mu\nu} - \frac{\varepsilon_2}{2}\, F^{(\theta)}_{\mu\nu} W^{3\,\mu\nu} + g_\theta A_{\theta\mu} J^\mu_\theta + \mathcal{L}_{\mathrm{SM}}. \quad (20)$$

Unitary gauge ($\Theta = 0$): $m_\theta = g_\theta f_\theta$, hence $\lambda_\theta = 1/m_\theta$.

7.3 Distance-law modifications with a shared range λ_θ

Massive spin-1 exchange between static sources (Born approximation): $V(r) = \mathrm{sgn}(Q_a Q_b)\,\frac{|g_a g_b|}{4\pi}\,\frac{e^{-m_\theta r}}{r}$. Gravity (fifth force): $V_G(r) = -\frac{G m_1 m_2}{r}[1 + \alpha_G e^{-r/\lambda_\theta}]$ with $\alpha_G = (g_\theta^2\beta^2)/(4\pi G)$ if $Q_\theta = \beta m$. QED (kinetic mixing): $V_{\mathrm{EM}}(r) = \alpha Q_1 Q_2/r + \varepsilon^2 \alpha Q_1 Q_2 e^{-r/\lambda_\theta}/r$.

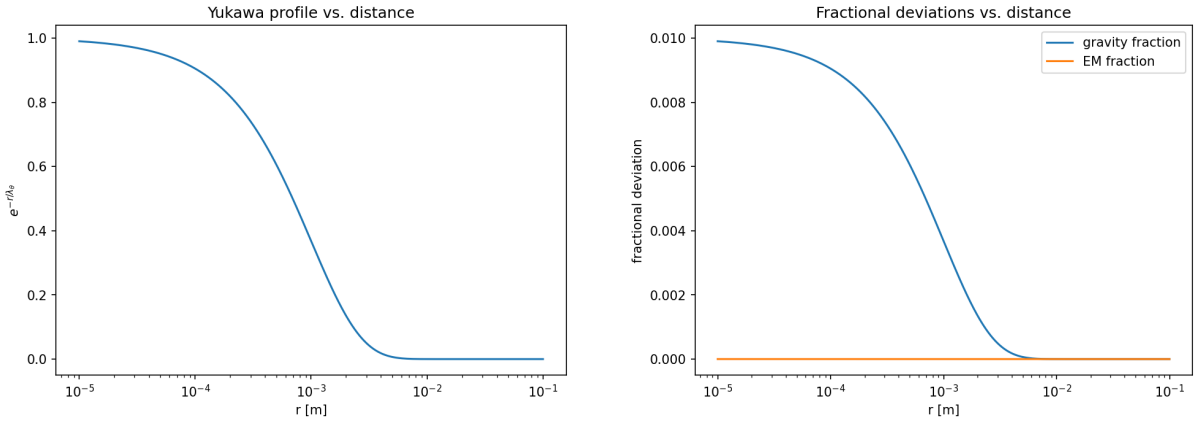

(a) Yukawa profile $V(r)$

(b) Fractional deviation vs distance

Figure 12: Shared-range λ_θ across sectors.

8 Notation & Symbols (quick lookup)

- Base coordinates: X^μ (or $X \in \mathbb{R}^3$ in NR limit); fiber: $\theta \in S^1$.
- Potentials: A_μ, A_θ; scalar potential $\phi \equiv A_0$.
- Curvatures: $G_{\mu\nu} = \partial_\mu A_\nu - \partial_\nu A_\mu$, $G_{\mu\theta} = \partial_\mu A_\theta - \partial_\theta A_\mu$.
- Charges: q_X (base $U(1)$), q_θ (fiber $U(1)$). Inertia: I.
- Holonomy: $\phi_\theta \equiv (q_\theta/\hbar) \oint A_\theta d\theta$.
- FRW: a, k, Σ^2; mode index ℓ; conserved Π_θ.

Glossary & Notation (Quick Reference)

Q Configuration space: $Q = \mathbb{R}^{3,1} \times S^1$ with coordinates $q^a = (X^\mu, \theta)$; θ is 2π-periodic.

θ Compact internal angle (the "dial"). Motion $\dot\theta$ is along the fiber, not in real space.

Compact S^1 The compact dimension; an angle with period 2π.

- **Analogy:** garden hose looks 1D from afar, but has a circular cross-section up close.

A **(connection)** Gauge connection 1-form on Q: $A = A_a\, dq^a = A_\mu\, dX^\mu + A_\theta\, d\theta$.

- **Analogy:** navigation tool that keeps phase transport consistent.

A_θ Internal gauge potential along θ; units $[A_\theta] = \hbar/q_\theta$ so $q_\theta A_\theta$ carries momentum.

A_μ, ϕ, $\mathbf{B}$ Spatial-temporal potential $A_\mu = (\phi, \mathbf{A})$ with $\phi \equiv A_0$ and $\mathbf{B} = \nabla \times \mathbf{A}$.

$G = dA$ Curvature (field strength) 2-form with components $G_{ab} = \partial_a A_b - \partial_b A_a$; measures loop holonomy.

$G_{\mu\theta}$ Mixed curvature: $G_{\mu\theta} = \partial_\mu A_\theta - \partial_\theta A_\mu$; in gauge $\partial_\theta A_\mu = 0$, $G_{i\theta} = \partial_i A_\theta$.

- **Analogy:** meshed gears; motion in one axis drives the other.

ϕ_θ Effective flux: $\phi_\theta \equiv \frac{q_\theta}{\hbar} \oint A_\theta\, d\theta$; physics is mod 2π.

Holonomy Loop-induced phase; for the fiber it is ϕ_θ above. Only ϕ_θ (mod 2π) is observable.

- **Analogy:** compass twist after hiking a closed loop.

Cross-Hall drift Sideways drift $\propto \partial_i A_\theta$ (i.e., $G_{i\theta}$) when the fiber potential varies across space; appears even for $\mathbf{E} = \mathbf{B} = 0$.

Rotor (internal) θ-motion behaves like a rotor with levels $E_\ell = \frac{\hbar^2}{2I}\left(\ell - \frac{\phi_\theta}{2\pi}\right)^2$, spacing $\Delta E \approx \hbar^2/(2I)$.

I Rotor (phase) inertia controlling sideband spacing $\Delta E \approx \hbar^2/(2I)$; NR map $I = m\kappa^2$.

- **Analogy:** heavier flywheel $\Rightarrow$ closer level spacing.

$m_\theta,\ \lambda_\theta$ Stückelberg mediator mass $m_\theta = g_\theta f_\theta$; Yukawa range $\lambda_\theta \equiv 1/m_\theta$.

Σ^2 Positive shear-like contribution $\propto a^{-6}$ in H^2 (early-time).

$q_X,\ q_\theta$ Charges coupling to A_μ and A_θ; minimal coupling $\mathbf{p} \to \mathbf{p} - q_X\mathbf{A}$, $p_\theta \to p_\theta - q_\theta A_\theta$.

Large gauge Large θ-loop: $\oint A_\theta d\theta \to \oint A_\theta d\theta + 2\pi\,\hbar/q_\theta$; only ϕ_θ modulo 2π is physical.

Einbein $e(\tau)$ Worldline multiplier ensuring reparametrization invariance; varying it imposes the mass-shell constraint; identifies $I = m\kappa^2$.

9 Related Work & Originality

I keep detailed comparisons (e.g., Kaluza–Klein, dark photon) concise here and emphasize what is original: a shared-range λ_θ cross-sector test, θ–AB at null EM, curvature-assisted bounce with WDW barrier, and the compact-fiber vacuum lever.

Comparative Analysis with Existing Frameworks

10 Vacuum Energy in X–θ: From Knife-Edge to Relaxation

Sketch of how the compact fiber can modify vacuum contributions; a full treatment is reserved for future work.

Data & Code Availability

All figure data are provided as CSV in `../paper/data/` and raster/vector figures in `../paper/figs/`.
Repository (simulation notebooks and build scripts): github.com/divyang4481/X-theta-framework.
Example links used in this paper: `../paper/data/exp1_theta_ab_fringe.csv`, `../paper/data/exp2_drift_`
`../paper/data/exp3_rotor_levels.csv`, `../paper/data/exp4_bounce_scan.csv`, `../paper/data/exp5_yu`

Correspondence: `22f1000411@ds.study.iitm.ac.in`; `divyang4481@gmail.com`

Table 1: Contrast of X–θ with Kaluza–Klein (KK) and String Theory (ST).

	X–θ	**Kaluza–Klein**	**String Theory**
Extra structure	1D *fiber* angle θ over spacetime; lab–programmable holonomy	Extra spatial dimensions compactified (fixed geometry)	10D/11D with compactification; rich moduli
Gauge origin	$U(1)_\theta$ with Stückelberg mass m_θ	Gauge from higher–dimensional metric components	Gauge from world-sheet/brane symmetries
Lab falsifiability	Direct: θ–AB, T^2 drift, rotor sidebands	Indirect: KK masses typically far above lab scales	Mostly high scale; low–energy windows are model dependent
Single–range test	Yes: one λ_θ across gravity/EM/weak	No single universal short range	Not generally a single range
Cosmo hook	Stiff a^{-6} + WDW barrier, bounce scale tied to lab I	Exotic matter from geometry; no simple lab knob	Early–universe from string cosmology; many scenarios
EP hygiene	$Q_\theta \propto m$ or $B\ell L \Rightarrow$ leading EP–safe	Composition dependence model–dependent	Model–dependent

Appendix A — Cross-Hall Drift Coefficient (paraxial beam)

Assuming a paraxial Gaussian $\psi(X,\theta,t) = \Phi(X,t)\,\chi(\theta,t)$ and slowly varying $A_\theta(X)$ across waist w_0, treating $G_{i\theta} = \partial_i A_\theta$ as uniform and linearizing the moments gives

$$\frac{d^2}{dt^2}\langle X_i\rangle = \frac{q_\theta}{m}\,(\partial_i A_\theta)\,\langle\dot\theta\rangle + \mathcal{O}(w_0^{-2}, \partial_i^2 A_\theta), \tag{21}$$

so a square gate of duration T yields $\Delta X_i = \alpha\,\frac{q_\theta}{m}\,(\partial_i A_\theta)\,\frac{T^2}{2}\,\langle\dot\theta\rangle$ with $\alpha \approx 1$ (top-hat) and $\alpha < 1$ (Gaussian).

Appendix B — Glossary

Holonomy Loop-induced phase from parallel transport around the fiber:

$$\Delta\varphi_\theta = \frac{q_\theta}{\hbar}\oint A_\theta\,d\theta \equiv \phi_\theta \pmod{2\pi}.$$

- **Analogy:** hiking a loop around a hill and finding your compass rotated when you return.
- **Where:** section 3.1.

Mixed curvature $G_{\mu\theta}$ Coupling between base and fiber:

$$G_{\mu\theta} = \partial_\mu A_\theta - \partial_\theta A_\mu, \quad \text{with } \partial_\theta A_\mu = 0 \Rightarrow G_{i\theta} = \partial_i A_\theta.$$

- **Analogy:** a gear train linking forward motion and an internal wheel.
- **Where:** section 3.2.

Minisuperspace Truncated configuration space for homogeneous modes (e.g., (a,θ) in FRW).

- **Analogy:** a city map showing only two main avenues.
- **Where:** section 4.

Inverse-square barrier Repulsive $+C/a^2$ term in the Wheeler–DeWitt (WDW) equation, with threshold for essential self-adjointness at $\gamma \geq 3/4$ for $-\chi'' + \frac{\gamma}{a^2}\chi$. Here $C \propto \ell^2\hbar^2/I_0$.

- **Where:** section 4.3.

Phase stiffness / inertia I Sets rotor sideband spacing $\Delta E \approx \hbar^2/(2I)$. NR map: $I = m\kappa^2$.

- **Analogy:** a heavier flywheel has more closely spaced levels.
- **Where:** section 3.3.

Einbein $e(\tau)$ Worldline multiplier enforcing reparametrization invariance; varying it imposes the mass-shell constraint. In the relativistic map one finds $I = m\kappa^2$.

- **Where:** section 2.3.

Gauge connection A One-form on Q that tracks phase transport: $A = A_\mu\, dX^\mu + A_\theta\, d\theta$, with curvature $G = dA$.

- **Analogy:** navigating a boat with changing currents.
- **Where:** section 2.4.

Compact dimension S^1 Fiber coordinate θ is an angle with period 2π.

- **Analogy:** a garden hose looks 1D from far away but has a circular cross-section up close.
- **Where:** section 2.

Flux quanta and large gauge The $U(1)_\theta$ flux quantum is $\Phi_{\theta,0} = 2\pi\hbar/q_\theta$; large θ-loops shift $\oint A_\theta d\theta$ by $2\pi\hbar/q_\theta$, so only ϕ_θ modulo 2π is physical.

- **Where:** section 2.4.

Rotor (internal) and sidebands With $\psi \sim e^{i\ell\theta}$, levels are

$$E_\ell = \frac{\hbar^2}{2I}\Big(\ell - \frac{\phi_\theta}{2\pi}\Big)^2, \quad \ell \in \mathbb{Z},$$

giving near-harmonic sidebands spaced by $\Delta E \approx \hbar^2/(2I)$.

- **Where:** section 3.3.

Stueckelberg mass m_θ **and Yukawa range** λ_θ In 4D, $m_\theta = g_\theta f_\theta$ and $\lambda_\theta \equiv 1/m_\theta$. The same λ_θ controls short-range fingerprints across gravity/QED/weak sectors.

- **Where:** section 7.

Kinetic mixing ε $U(1)$–$U(1)$ mixing induces a small Yukawa bump in Coulomb's law.

- **Analogy:** two pendulums tied by a weak spring.
- **Where:** section 7.

Cross-Hall drift Transverse drift proportional to $\partial_i A_\theta$ when the fiber potential varies across space; see also Appendix 10 for a paraxial coefficient.

- **Where:** section 3.2.

Charges $q_X,\ q_\theta$ Minimal coupling rules: $\mathbf{p} \to \mathbf{p} - q_X\mathbf{A}$ and $p_\theta \to p_\theta - q_\theta A_\theta$.

- **Where:** section 2.

References

[1] Wikipedia contributors. Quantum mechanics. https://en.wikipedia.org/wiki/Quantum_mechanics, 2023. Accessed: 2025-09-12.

[2] Wikipedia contributors. General relativity. https://en.wikipedia.org/wiki/General_relativity, 2023. Accessed: 2025-09-12.

[3] Richard P. Feynman. Feynman's double slit experiment. YouTube, https://www.youtube.com/watch?v=DfPeprQ7oGc, 2011. Accessed: 2025-09-12.

[4] Albert Einstein. Einstein's nobel lecture: The photoelectric effect. Nobel Prize Archive, https://www.nobelprize.org/prizes/physics/1921/einstein/lecture/, 1921. Accessed: 2025-09-12.

[5] T. Padmanabhan. The cosmological constant and the vacuum energy crisis. arXiv:astro-ph/0005265, https://arxiv.org/abs/astro-ph/0005265, 2000. Accessed: 2025-09-12.

[6] V. Balakrishnan. Quantum physics lectures (nptel, iit madras). Lecture series, 2013. Accessed 11 Sep 2025.

[7] B. Holdom. Two u(1)'s and epsilon charge shifts. *Phys. Lett. B*, 166:196–198, 1986.

[8] L. Okun. Limits of electrodynamics: Paraphotons? *Sov. Phys. JETP*, 56:502, 1982.

[9] R. Essig et al. Dark sectors and new, light, weakly-coupled particles. *arXiv preprint*, 2013.

[10] Y. Aharonov and D. Bohm. Significance of electromagnetic potentials in the quantum theory. *Phys. Rev.*, 115:485–491, 1959.

[11] A. Tonomura et al. Observation of aharonov–bohm effect by electron holography. *Phys. Rev. Lett.*, 56:792, 1986.

[12] M. V. Berry. Quantal phase factors accompanying adiabatic changes. *Proc. R. Soc. Lond. A*, 392:45–57, 1984.

[13] F. Wilczek and A. Zee. Appearance of gauge structure in simple dynamical systems. *Phys. Rev. Lett.*, 52:2111, 1984.

[14] Jean Dalibard, Fabrice Gerbier, Gediminas Juzeliūnas, and Patrik Öhberg. Colloquium: Artificial gauge potentials for neutral atoms. *Rev. Mod. Phys.*, 83:1523–1543, 2011.

[15] N. Goldman, G. Juzeliūnas, P. Öhberg, and I. B. Spielman. Light-induced gauge fields for ultracold atoms. *Rep. Prog. Phys.*, 77(12):126401, 2014.

[16] N. F. Ramsey. A molecular beam resonance method with separated oscillating fields. *Phys. Rev.*, 78:695, 1950.

[17] H. Rauch et al. Verification of coherent spinor rotation of fermions. *Phys. Lett. A*, 54:425, 1975.

[18] S. A. Werner et al. Observation of the phase shift of a neutron due to precession in a magnetic field. *Phys. Rev. Lett.*, 35:1053, 1975.

[19] H. Ruegg and M. Ruiz-Altaba. The stückelberg field. *Int. J. Mod. Phys. A*, 19:3265, 2004.

[20] M. Fabbrichesi, E. Gabrielli, and G. Lanfranchi. *The Dark Photon*. SpringerBriefs in Physics, 2020.

[21] A. Berlin et al. Dark photons and experimental probes. *Rev. Mod. Phys.*, 94:015003, 2022.

[22] Theodor Kaluza. Zum unitätsproblem der physik. *Sitzungsberichte der Preussischen Akademie der Wissenschaften*, pages 966–972, 1921.

[23] Oskar Klein. Quantum theory and five-dimensional relativity. *Zeitschrift für Physik*, 37:895–906, 1926.

[24] Max Born and Leopold Infeld. Foundations of the new field theory. *Proc. R. Soc. A*, 144:425–451, 1934.

[25] Máximo Bañados and Pedro G. Ferreira. Eddington's theory of gravity and its progeny. *Phys. Rev. Lett.*, 105:011101, 2010.

[26] P. P. Avelino. Eddington-inspired born–infeld gravity: Astrophysical and cosmological constraints. *Phys. Rev. D*, 85:104053, 2012.

[27] Abhay Ashtekar, Tomasz Pawlowski, and Parampreet Singh. Quantum nature of the big bang: Improved dynamics. *Phys. Rev. D*, 74:084003, 2006.

[28] Iván Agulló and Parampreet Singh. Loop quantum cosmology. In *Loop Quantum Gravity: The First 30 Years*. World Scientific, 2017. chapter-length review.

[29] Leonardo Modesto. Black hole interior from loop quantum gravity. *Advances in High Energy Physics*, page 459290, 2008.

[30] Hugo A. Morales-Técotl et al. Effective dynamics of the schwarzschild black hole interior in loop quantum gravity. *arXiv:1806.05795*, 2018.

[31] Mehdi Assanioussi, Andrea Dapor, and Klaus Liegener. Perspectives on the dynamics in a loop quantum gravity effective description of black hole interiors. *Phys. Rev. D*, 101:026002, 2020.

[32] Yakir Aharonov and David Bohm. Significance of electromagnetic potentials in the quantum theory. *Phys. Rev.*, 115:485–491, 1959.

[33] D. J. Stargen et al. Polymer quantization and advanced gravitational-wave detector. *Phys. Rev. D*, 100:086007, 2019.

[34] Nirmalya Kajuri. Low-energy lorentz violation in polymer quantization. *arXiv:1711.08234*, 2017.

[35] Marco Fabbrichesi, Emidio Gabrielli, and Gaia Lanfranchi. The dark photon. *arXiv:2005.01515*, 2020. Comprehensive review.

[36] Amina Berkane and Mounir Boussahel. Dark photon as an extra u(1) extension to the standard model with general rotation in kinetic mixing. *arXiv:2101.03689*, 2021.